SMEFT Analysis of m_W

Emanuele Bagnaschi,[a] **John Ellis,**[b,a,c] **Maeve Madigan,**[d] **Ken Mimasu,**[b]
Veronica Sanz[e,f] **and Tevong You**[a,b,d,g]

[a] *Theoretical Physics Department, CERN, CH-1211 Geneva 23, Switzerland*

[b] *Theoretical Particle Physics and Cosmology Group, Department of Physics,*
King's College London, London WC2R 2LS, UK

[c] *National Institute of Chemical Physics & Biophysics, Rävala 10, 10143 Tallinn, Estonia*

[d] *DAMTP, University of Cambridge, Wilberforce Road, Cambridge CB3 0WA, UK*

[e] *Instituto de Física Corpuscular (IFIC), Universidad de Valencia-CSIC, E-46980 Valencia, Spain*

[f] *Department of Physics and Astronomy, University of Sussex, Brighton BN1 9QH, UK*

[g] *Cavendish Laboratory, University of Cambridge, J.J. Thomson Avenue, Cambridge CB3 0HE,*
UK

E-mail: emanuele.bagnaschi@cern.ch, john.ellis@cern.ch,
mum20@cam.ac.uk, ken.mimasu@kcl.ac.uk, veronica.sanz@uv.es,
tevong.you@cern.ch

ABSTRACT: We use the `Fitmaker` tool to incorporate the recent CDF measurement of m_W in a global fit to electroweak, Higgs, and diboson data in the Standard Model Effective Field Theory (SMEFT) including dimension-6 operators at linear order. We find that including any one of the SMEFT operators $\mathcal{O}_{HWB}$, $\mathcal{O}_{HD}$, $\mathcal{O}_{\ell\ell}$ or $\mathcal{O}_{H\ell}^{(3)}$ with a non-zero coefficient could provide a better fit than the Standard Model, with the strongest pull for $\mathcal{O}_{HD}$ and no tension with other electroweak precision data. We then analyse which tree-level single-field extensions of the Standard Model could generate such operator coefficients with the appropriate sign, and discuss the masses and couplings of these fields that best fit the CDF measurement and other data. In particular, the global fit favours either a singlet Z' vector boson, a scalar electroweak triplet with zero hypercharge, or a vector electroweak triplet with unit hypercharge, followed by a singlet heavy neutral lepton, all with masses in the multi-TeV range for unit coupling.

Contents

1 Introduction

The Standard Model Effective Field theory (SMEFT) provides a powerful framework for analysing possible experimental deviations from Standard Model (SM) predictions that could be due to new physics with an energy scale Λ above those explored directly by current experiments [1, 2]. The leading SMEFT contributions to experimental observables appear in linear order, and are due to interferences between SM amplitudes and those generated by dimension-6 operators. A global analysis of such linear SMEFT effects in electroweak, Higgs, diboson and top data using the `Fitmaker` tool found consistency with the SM and no significant evidence for new physics from measurements made during run 2 of the LHC and by previous experiments [3]. [1] The SMEFiT collaboration subsequently made a global analysis that included SMEFT effects at quadratic order [7], assuming that the precision electroweak data are consistent with the SM. Other global fits have been performed for various combinations of electroweak, diboson and Higgs data, e.g., [8–15], as well as separate fits to mainly top measurements, e.g., [16–27].

An exciting recent development has been a measurement of the W-boson mass, m_W, by the CDF Collaboration [28], which found $m_W = 80433.5 \pm 9.4$ MeV. This value is in significant tension with the SM prediction obtained from precision electroweak data, namely $m_W = 80354 \pm 7$ MeV [33], and also previous direct measurements including the most precise one, that by the ATLAS Collaboration, $m_W = 80370 \pm 19$ MeV [36], as seen in Fig. 1. Pending future scrutiny and resolution of its tension with previous measurements, here we accept the CDF experimental result at face value, and use the SMEFT at linear order

---

[1]More recently, some evidence for new physics has been found in measurements of flavour observables (see [4] and references therein) and the anomalous magnetic moment of the muon [5, 6], but we do not discuss those phenomena here.
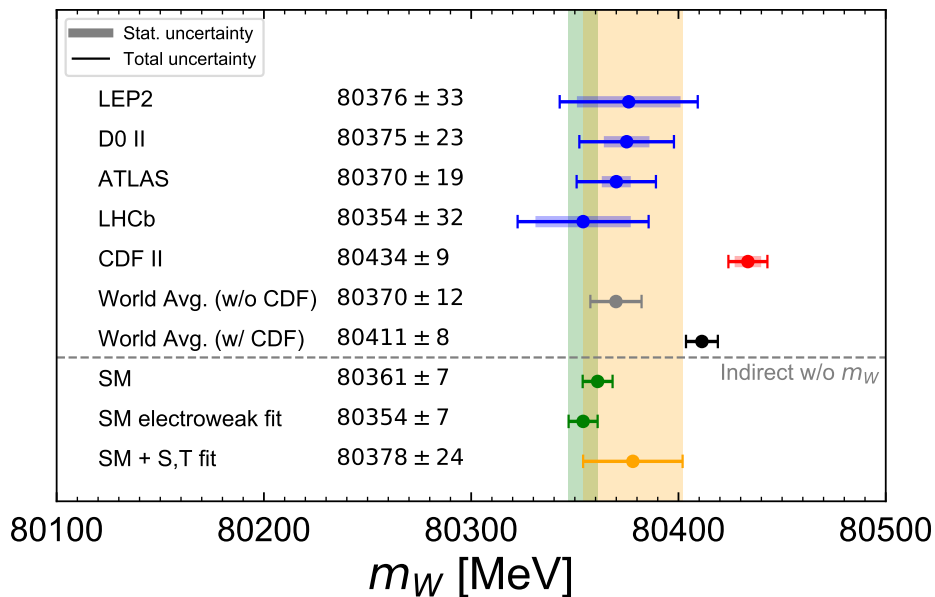
Figure 1. *A comparison of the new CDF measurement of m_W (red) [28] with previous measurements (blue) [29–31], and a naive world average with (black) and without (grey) CDF. The values found in the Standard Model using fixed input parameters [32], or determined from an electroweak fit omitting measurements of m_W [33], are shown in green. The orange band is the 1-σ range allowed in a two-parameter fit to the oblique electroweak precision parameters S and T [34, 35] made using the SMEFT operators $\mathcal{O}_{HWB}$ and $\mathcal{O}_{HD}$ in* Fitmaker, *also omitting any direct measurement of m_W.*

in dimension-6 operator coefficients to explore its potential implications for new physics beyond the Standard Model.

There have been previous indications from LEP, Tevatron and ATLAS that m_W might be slightly larger than the SM prediction from an electroweak fit to the SM that omits the m_W measurements [33], shown as the green band in Fig. 1. A recent measurement by LHCb [31] brought down the world average of direct measurements, though its uncertainty remained relatively large. A world average obtained by taking the combination of LEP results with D0 and CDF was given by CDF in [28]. Fig. 1 shows in black (grey) the result of the ATLAS and LHCb measurements combined with (omitting) the new CDF measurement neglecting correlations, displaying the apparent tension with the SM. Some tension was evident already before the CDF measurement, and may remain even in the event that additional uncertainties are identified. Identifying new physics able to mitigate this tension and quantifying its consistency with other data provides a theoretical perspective that is complementary to the experimental one.

There have been many theoretical studies of the possibility of a deviation of m_W from its SM value, e.g., in the context of extensions of the SM such as supersymmetry. However, a deviation as large as that reported by CDF is difficult to obtain with electroweak sparticles in a minimal supersymmetric model (see [37] and references therein). More generically,

new physics parametrised by the oblique parameters S and T [34, 35] could accommodate a sizeable enhancement of m_W while remaining compatible with electroweak precision data, as shown by the orange band in Fig. 1. This was obtained by using `Fitmaker` to make a fit including the SMEFT operators $\mathcal{O}_{HWB}$ and $\mathcal{O}_{HD}$ and omitting direct m_W measurements.

The main purpose of this paper is to present global fits in the general and relatively model-independent framework provided by the SMEFT, exploring the extent to which it can accommodate the CDF result and other measurements of m_W and, if so, in what type of minimal extension of the SM might be rersponsible. We identify several suitable single-field extensions of the SM that can accommodate the CDF measurement and other measurements, and estimate the favoured ranges of the masses of the new particles, finding that they may well be sufficiently heavy for our leading-order SMEFT analysis to be consistent. We also comment on the prospects for direct LHC searches for these new particles. We note that the PDG has proposed [32] a prescription for combining data that are only poorly consistent, and we comment on the changes in our final results if the experimental uncertainties in Fig. 1 are rescaled using this prescription.

The CDF anomaly requires confirmation. Nevertheless, our SMEFT analysis of M_W uncovers flat directions and highlights the complementarity of different datasets in constraining the multi-dimensional space of Wilson coefficients, as well as the UV extensions that they probe. Our M_W analysis represents a first step towards extending our previous SMEFT analysis to include constraints from CKM unitarity, and provides a useful guide for future phenomenological studies of models that were motivated by measurements of M_W even prior to the CDF measurement [37–40].

2 m_W in the SMEFT

The SMEFT Lagrangian for dimension-6 operators $\mathcal{O}_i$ has coefficients normalised as

$$\mathcal{L}_{\text{SMEFT}}^{\text{dim-6}} = \sum_{i=1}^{2499} \frac{C_i}{\Lambda^2} \mathcal{O}_i \,, \tag{2.1}$$

where the C_i are dimensionless Wilson coefficients and Λ represents a dimensionful scale. The number of operators is reduced in our fit [3] by assuming a $SU(3)^5$ flavour symmetry. At linear order, four dimension-6 SMEFT operators can induce a shift in the W mass, namely

$$\mathcal{O}_{HWB} \equiv H^\dagger \tau^I H \, W_{\mu\nu}^I B^{\mu\nu}, \quad \mathcal{O}_{HD} \equiv \left(H^\dagger D^\mu H \right)^\star \left(H^\dagger D_\mu H \right) \,,$$
$$\mathcal{O}_{\ell\ell} \equiv \left(\bar{\ell}_p \gamma_\mu \ell_r \right) \left(\bar{\ell}_s \gamma^\mu \ell_t \right) \,, \quad \mathcal{O}_{H\ell}^{(3)} \equiv \left(H^\dagger i \overleftrightarrow{D}_\mu^I H \right) \left(\bar{\ell}_p \tau^I \gamma^\mu \ell_r \right) \,, \tag{2.2}$$

where we adopt the Warsaw basis [41] for these and other dimension-6 SMEFT operators. The pole mass shift relative to the SM is given by

$$\frac{\delta m_W^2}{m_W^2} = -\frac{\sin 2\theta_w}{\cos 2\theta_w} \frac{v^2}{4\Lambda^2} \left(\frac{\cos \theta_w}{\sin \theta_w} C_{HD} + \frac{\sin \theta_w}{\cos \theta_w} \left(4C_{Hl}^{(3)} - 2C_{ll} \right) + 4C_{HWB} \right) . \tag{2.3}$$
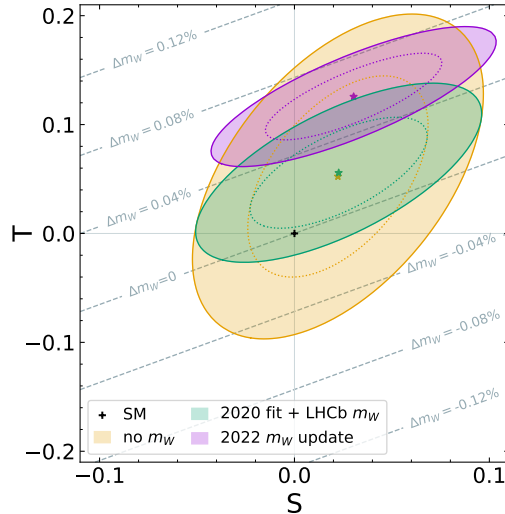
Figure 2. *The 68% and 95% CL contours of fits to the oblique parameters S and T, which are equivalent to a fit including the SMEFT operators $\mathcal{O}_{HWB}$ and $\mathcal{O}_{HD}$, see Eq. (2.5). The orange, green, and purple contours are the result of fits omitting m_W measurements, with m_W previous to the recent CDF measurement, and including the latest CDF result. We see a clear pull away from the SM value at the origin due to the CDF result, which nevertheless remains compatible with the range allowed by other data. The percentage shifts in the W mass are denoted by dashed grey lines.*

We use the electroweak input scheme that uses $\{\alpha_{EW}, G_F, M_Z\}$ as input parameters [42], with values

$$\alpha_{EW}^{-1} = 127.95 \quad , \quad G_F = 1.16638 \times 10^{-5} \text{ GeV}^{-2} \quad , \quad m_Z = 91.1876 \text{ GeV}. \qquad (2.4)$$

We neglect in our fit theoretical SMEFT errors such as a possible measurement bias in extracting the value of m_W in the SMEFT, which has been shown to be negligible [43].

A common parametrisation of new physics involves the oblique parameters S and T [34, 35], which can indicate the range of m_W allowed by electroweak precision observables under the assumption of this 2-parameter framework. Their relation to the dimension-6 SMEFT operators in the Warsaw basis is given by

$$\frac{v^2}{\Lambda^2}C_{HWB} = \frac{g_1 g_2}{16\pi}S \quad , \quad \frac{v^2}{\Lambda^2}C_{HD} = -\frac{g_1^2 g_2^2}{2\pi(g_1^2 + g_2^2)}T. \qquad (2.5)$$

Before going into the details of our global SMEFT fit in the next Section, we show in Fig. 2 the 68% and 95% CL contours of fits to S and T. The orange, green, and purple contours are the result of a fit omitting m_W measurements, with m_W prior to CDF's update, and including the latest CDF determination. We see a clear pull away from the SM value at the origin due to the CDF result, which nevertheless remains compatible with the range allowed by the data without m_W. Contours of the percent shift in m_W are shown as dashed grey lines, with an enhancement of Δm_W from 0.04% to 0.08% being favoured.

In the next Section we discuss the compatibility of the CDF result with the complete set of electroweak, Higgs and diboson data within the more general SMEFT framework.

SMEFT Coeff.	Individual			Marginalised		
	Best fit [Λ = 1 TeV]	95% CL range	Scale $\frac{\Lambda}{\sqrt{C}}$ [TeV]	Best fit [Λ = 1 TeV]	95% CL range	Scale $\frac{\Lambda}{\sqrt{C}}$ [TeV]
C_{HWB}	-0.01	[-0.009, -0.0034]	19.0	0.25	[-0.3, +0.81]	1.3
C_{HD}	-0.03	[-0.035, -0.019]	11.0	-0.6	[-1.8, +0.63]	0.9
C_{ll}	0.02	[+0.014, +0.034]	10.0	-0.05	[-0.099, +0.0043]	4.4
$C_{Hl}^{(3)}$	-0.01	[-0.019, -0.0083]	14.0	-0.01	[-0.11, +0.076]	3.3
$C_{Hl}^{(1)}$	0.00	[-0.0045, +0.013]	11.0	0.16	[-0.15, +0.47]	1.8
C_{He}	0.00	[-0.015, +0.0071]	9.6	0.28	[-0.34, +0.9]	1.3
$C_{Hq}^{(3)}$	0.00	[-0.013, +0.011]	9.1	-0.05	[-0.11, +0.012]	4.1
$C_{Hq}^{(1)}$	0.01	[-0.027, +0.043]	5.4	-0.07	[-0.2, +0.06]	2.8
C_{Hd}	-0.03	[-0.13, +0.072]	3.1	-0.44	[-0.96, +0.079]	1.4
C_{Hu}	0.00	[-0.075, +0.073]	3.7	-0.18	[-0.62, +0.26]	1.5
C_{HBox}	-0.27	[-1, +0.47]	1.2	-1.1	[-3.2, +1]	0.69
C_{HG}	0.00	[-0.0034, +0.0032]	17.0	-0.01	[-0.026, +0.013]	7.2
C_{HW}	0.00	[-0.012, +0.006]	11.0	0.18	[-0.33, +0.7]	1.4
C_{HB}	0.00	[-0.0034, +0.002]	19.0	0.09	[-0.074, +0.24]	2.5
C_W	0.18	[-0.072, +0.42]	2.0	0.15	[-0.1, +0.4]	2.0
C_G	-0.75	[-4, +2.5]	0.56	1.3	[-6.1, +8.7]	0.37
$C_{\tau H}$	0.01	[-0.015, +0.025]	7.1	0.00	[-0.017, +0.027]	6.7
$C_{\mu H}$	0.00	[-0.0057, +0.005]	14.0	0.00	[-0.0056, +0.0052]	14.0
C_{bH}	0.00	[-0.016, +0.024]	7.1	0.02	[-0.027, +0.058]	4.8
C_{tH}	-0.09	[-1, +0.84]	1.0	-2.7	[-8.8, +3.3]	0.41

Table 1. *Table of the numerical results from the global fits to the electroweak, diboson and Higgs data in the CDF-friendly flavour-symmetric SU(3)[5] scenario that are visualised in Fig. 3, switching on only each individual operator (left columns) and including all operators and marginalising over the other operator coefficients (right columns).*
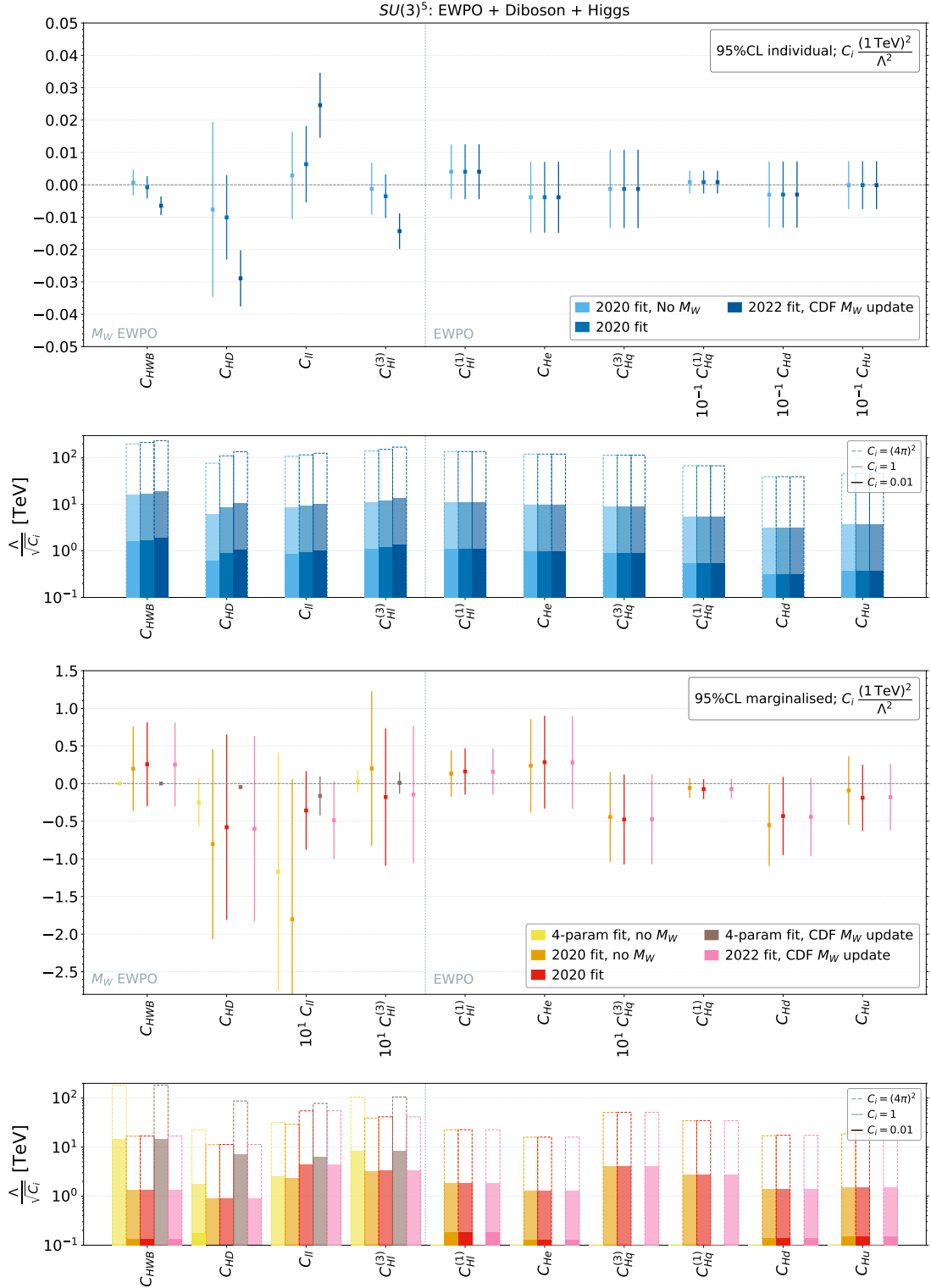
Figure 3. *Constraints from global linear fits to measurements of m_W combined with Higgs, diboson and electroweak precision observables made using* `Fitmaker` *[3] on the individual and marginalised operator coefficients $C_i(1\,\mathrm{TeV})^2/\Lambda^2$ (top and third panels, respectively) and the corresponding scales Λ for the indicated values of the dimensionless coupling C_i at the 95% confidence level (second and bottom panels). In the upper panels we compare results for the individual operators dropping the m_W constraint, using the m_W constraint applied in [3], and using the new CDF measurement of m_W. In the lower panels, we compare the constraints obtained marginalising either over the full set of 20 operators, or over the four operators that can modify m_W.*

3   SMEFT Fit Results

The `Fitmaker` tool [3] includes consistently all the linear (interference) effects of dimension-6 SMEFT operators. We use the same electroweak, Higgs and diboson data set as that analysed in [3], comparing with results obtained by incorporating the new CDF measurement of m_W [28]. We assume that the coefficients of the dimension-6 operators involving fermions are flavour-universal, i.e., imposing on them an $\mathrm{SU}(3)^5$ flavour symmetry and allowing a total of 20 operators in our analysis [2].

One would expect the preferred values of the coefficients of the four operators (2.2) of dimension 6 that can modify the SM prediction for m_W at the linear level, namely $C_{HWB,HD,\ell\ell}$ and $C_{H\ell}^{(3)}$, to be influenced by the inclusion of the CDF measurement of m_W in the global dataset. Indeed, we find this in global fits to individual operator coefficients: the upper panels of Fig. 3 show results for a subset of operators most constrained by electroweak precision observables. We see in the top panel that negative values of C_{HWB}, C_{HD} and $C_{H\ell}^{(3)}$ are preferred, but a positive value of $C_{\ell\ell}$. Comparing with the fit omitting the measurements of m_W and the fit including the old determination of m_W, the new best fit values remain compatible at the 95% CL while exhibiting a clear pull away from zero. The bars in the second panel show the sensitivities (i.e. the widths of the 95% CL uncertainties centred around zero) of the respective fits to the mass scales in the coefficients of the respective operators. The dark, light, and transparent shadings correspond to $C_i = 0.01, 1, (4\pi)^2$, respectively.

On the other hand, the effects of including the CDF measurement are less apparent in the lower panels of Fig. 3, where we display the weaker constraints on the operator coefficients obtained when either all operators are included in the fit and their coefficients are marginalised over, or just the four operators that contribute to m_W are included and marginalised over. Although results for only a subset of operators most strongly constrained in electroweak precision observables are displayed in Fig. 3, all the 20 operators are included in our flavour-universal $\mathrm{SU}(3)^5$ fit. The effect of m_W on the operators not displayed is negligible. We present in Table 1 our numerical results for the 20 $\mathrm{SU}(3)^5$-symmetric dimension-6 operator coefficients in the individual and fully marginalised fits when the CDF value of m_W is included.

We now turn to a comparison between indirect and direct measurements of the W mass to assess their compatibility when allowing for different combinations of operator coefficients. Fig. 4 displays the best fit value and 1-σ range of m_W in a variety of SMEFT fits to all combinations of operators entering linearly in m_W, including from 1 to 4 operator coefficients, as well as a fit to all 20 operator coefficients. The grey points represent the results omitting m_W from the SMEFT fit, while the red points are for the SMEFT fit including m_W. The green band is the SM prediction the input parameters shown in (2.4), and the yellow band is the current world average of m_W experimental measurements. Overlap of a grey uncertainty with a red one indicates compatibility at the 1-σ level of the latest

---

[2]Since the correlations between top sector operators and bosonic operators were shown in [3] to be relatively weak, we expect that including top data or making a fit in which operators involving top quarks break the flavour symmetry down to $\mathrm{SU}(2)^2 \times \mathrm{SU}(3)^2$ would yield similar results.
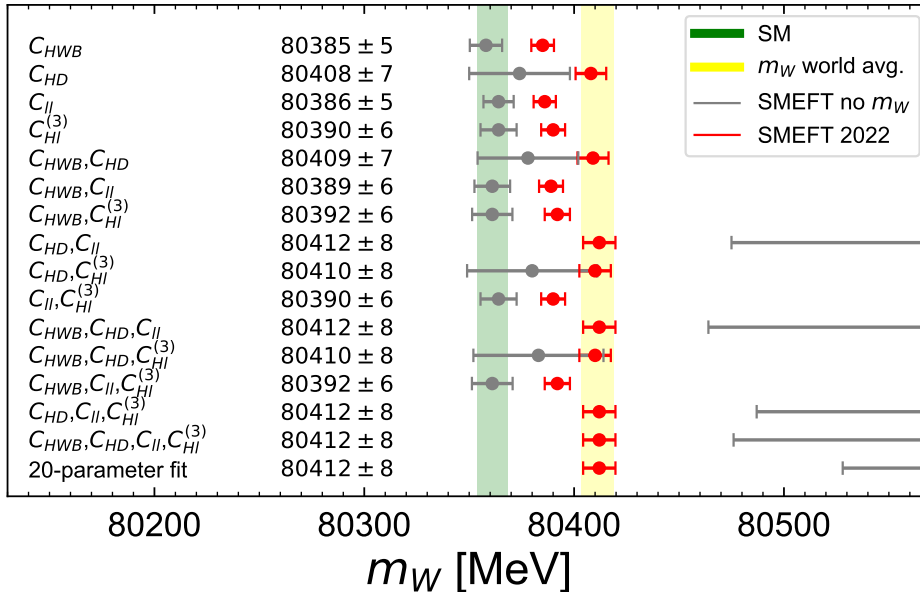
Figure 4. *Values of m_W in fits including all combinations of operators entering linearly in m_W, including from 1 to 4 operator coefficients, as well as a fit to 20 operator coefficients. Results omitting direct measurements of m_W are shown in grey, and results using the current world average of m_W measurements including that by CDF are shown in red. The vertical green band is the SM prediction for m_W based on other data, and the yellow band is the current world average of m_W measurements.*

updated fit with prior data excluding m_W. We see that, especially before including an m_W measurement, C_{HD} is the least constrained of the single-parameter scenarios, which enables any fit to subsets of operators involving C_{HD} to find a best fit value of m_W compatible with our world average determination. All other subsets excluding C_{HD} are more strongly constrained by data other than m_W and so have a best fit m_W that is pulled down accordingly. Finally, we note that subsets involving C_{HD} and C_{ll} together are pulled to much larger values with large uncertainties if the direct measurement of m_W is not included in the fit, indicating an almost flat direction that is lifted by the inclusion of m_W. Low-energy measurements sensitive to C_{ll} may also break this degeneracy. These have been studied, e.g., in Refs. [44, 45], but are currently not fully implemented in `Fitmaker`, though we study the impact of low-energy measurements related to unitarity of the CKM matrix in Appendix A.

We display in Fig. 5 the 68% and 95% CL constraints on pairs of the coefficients of operators capable of modifying m_W that are obtained in a fit using all measurements of m_W including that from CDF, by marginalising over the coefficients of the four operators that affect m_W (green), including just the two operators in each plane (purple), and comparing the results when omitting all m_W measurements (beige). We see in every plane that the 2-operator fit is more constraining than the 4-operator fit. The constraints also strengthen significantly when including m_W. In particular, a flat direction between C_{ll} and C_{HD} is
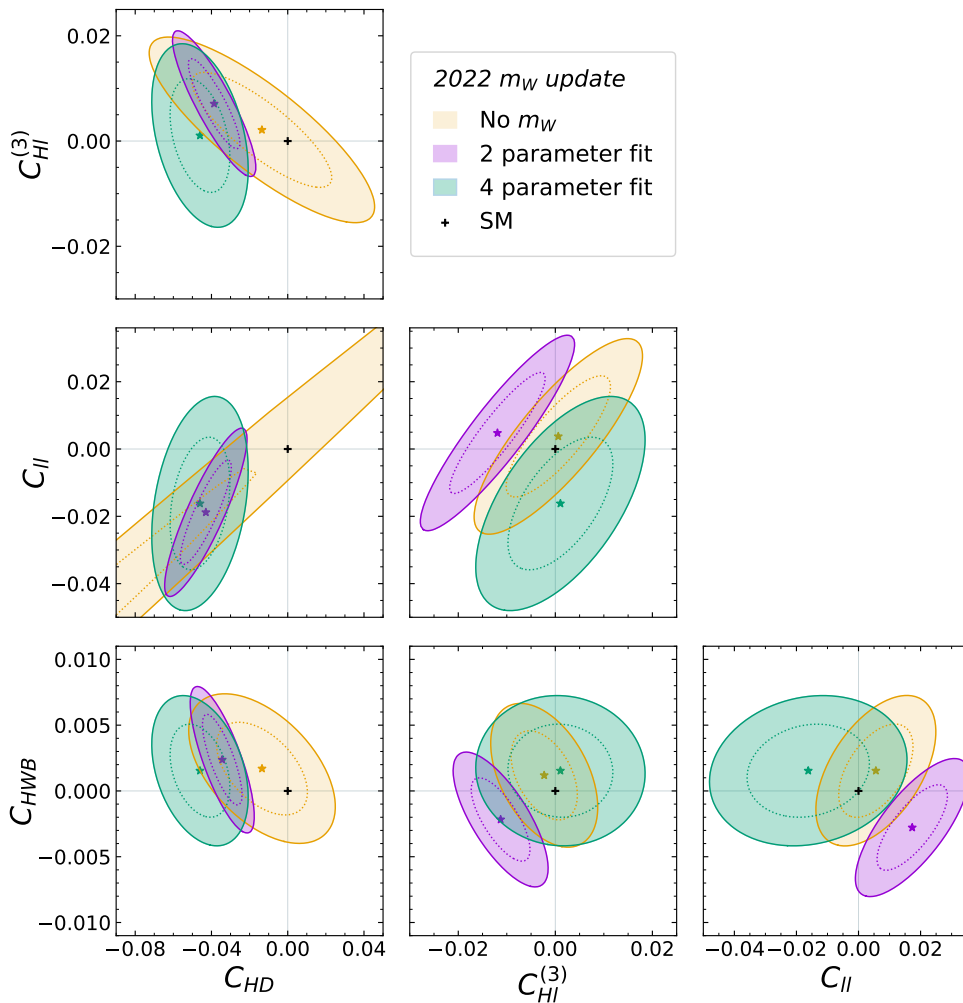
Figure 5. *Planes of pairs of the coefficients of operators that can affect m_W, comparing the constraints obtained when omitting m_W measurements from the fit (beige), marginalising over just the four operators that affect m_W (green), and marginalising over only the two operators in each plane (purple).*

lifted and we see that C_{HD} is bounded away from zero in each of the three planes where it features, whereas the other operator coefficients may be consistent with zero. However, the SM lies outside the parameter ellipses in all the planes involving C_{HD}.

4 Probing Single-Field Extensions of the Standard Model

We now analyse whether our fit favours any particular UV completions of the SM by analysing single-field extensions of the SM Lagrangian, updating the analysis presented in [3]. The single-field extensions of the SM that contribute to dimension-6 SMEFT operator coefficients at tree level have been catalogued in [46], and we list in Table 2 the models that can contribute to m_W. The expressions for the dimension-6 operator coefficients generated

by these single-field models at the tree-level are given in Table 3, which is taken directly from [46], assuming that only a single coupling to the Higgs is present. We focus here on tree-level extensions of the SM, since models modifying m_W at loop level are likely to involve particles below the TeV scale, for which the SMEFT approach is questionable.

There are no single-field models that contribute at tree level to C_{HWB}, and only S_1 contributes to $C_{\ell\ell}$. Three single-field models contribute to C_{HD}, and four to $C_{H\ell}^{(3)}$. In both of the latter cases, these single-field models also contribute to other operator coefficients, and their contributions vary between models. As we discuss below, these effects open up the possibility in principle of discriminating between the different CDF-friendly single-field extensions of the SM. We note that model S_1 generates a negative contribution to $C_{\ell\ell}$ (due to the antisymmetry of the S_1 Yukawa matrix in flavour space [47, 48]) whereas the data prefer a positive value, that Σ and Σ_1 generate positive contributions to $C_{H\ell}^{(3)}$ whereas the data prefer a negative value, and that models W and B_1 generate positive contributions to C_{HD} whereas the data again prefer a negative value. For this reason, these models do not improve on the SM fit. On the other hand, models N and E generate the preferred sign of $C_{H\ell}^{(3)}$ and models Ξ, B and W_1 generate the preferred sign of C_{HD}, so these models can improve on the SM fit.

Model	Spin	SU(3)	SU(2)	U(1)	Parameters
S_1	0	1	1	1	(M_S, κ_S)
Σ	$\frac{1}{2}$	1	3	0	$(M_\Sigma, \lambda_\Sigma)$
Σ_1	$\frac{1}{2}$	1	3	-1	$(M_{\Sigma_1}, \lambda_{\Sigma_1})$
N	$\frac{1}{2}$	1	1	0	(M_N, λ_N)
E	$\frac{1}{2}$	1	1	-1	(M_E, λ_E)
B	1	1	1	0	$(M_B, \hat{g}_H^B)$
B_1	1	1	1	1	(M_{B_1}, λ_{B_1})
Ξ	0	1	3	0	(M_Ξ, κ_Ξ)
W_1	1	1	3	1	$(M_{W_1}, \hat{g}_{W_1}^\varphi)$
W	1	1	3	0	$(M_W, \hat{g}_W^H)$

Table 2. *The single-field extensions listed in the first column can make tree-level contributions to m_W. They have the quantum numbers listed in the following three columns, and the notations for their masses and couplings are given in the last column.*

Fig. 6 displays the constraints we find on the single-field extensions of the SM catalogued in Table 2 that can increase m_W above its SM value. The salmon and ochre bars show the preferred mass ranges (in TeV) for these models at the 68% and 95% CL, respectively, setting the corresponding model couplings to unity. The mass ranges would scale linearly with the magnitudes of the couplings. Numerical results are collected in Table 4, where we also quote the 68% CL ranges of the couplings assuming that the masses of the additional field are 1 TeV. The rows of the Table are ordered according to decreasing values of the pulls. In the case of the Ξ field, the relevant coupling, κ_Ξ, has dimensions of mass, which explains the additional factor of M_Ξ^{-2} in the corresponding entries of Table 3. Here we have

Model	C_{HD}	C_{ll}	$C_{Hl}^{(3)}$	$C_{Hl}^{(1)}$	C_{He}	$C_{H\Box}$	$C_{\tau H}$	C_{tH}	C_{bH}
S_1		-1							
Σ			$\frac{1}{16}$	$\frac{3}{16}$			$\frac{y_\tau}{4}$		
Σ_1			$\frac{1}{16}$	$-\frac{3}{16}$			$\frac{y_\tau}{8}$		
N			$-\frac{1}{4}$	$\frac{1}{4}$					
E			$-\frac{1}{4}$	$-\frac{1}{4}$			$\frac{y_\tau}{2}$		
B_1	1					$-\frac{1}{2}$	$-\frac{y_\tau}{2}$	$-\frac{y_t}{2}$	$-\frac{y_b}{2}$
B	-2						$-y_\tau$	$-y_t$	$-y_b$
Ξ	$-2\left(\frac{1}{M_\Xi}\right)^2$					$\frac{1}{2}\left(\frac{1}{M_\Xi}\right)^2$	$y_\tau\left(\frac{1}{M_\Xi}\right)^2$	$y_t\left(\frac{1}{M_\Xi}\right)^2$	$y_b\left(\frac{1}{M_\Xi}\right)^2$
W_1	$-\frac{1}{4}$					$-\frac{1}{8}$	$-\frac{y_\tau}{8}$	$-\frac{y_t}{8}$	$-\frac{y_b}{8}$
W	$\frac{1}{2}$					$-\frac{1}{2}$	$-y_\tau$	$-y_t$	$-y_b$

Table 3. *Operators generated at the tree level by the single-field extensions listed in the first column, which can make tree-level contributions to m_W. The coefficients of the operators are given by the squares of the corresponding coupling divided by the corresponding M^2, with the exception of an extra factor of $1/m_\Xi^2$ in the case of the Ξ field, as noted in the Table. We denote the top, bottom and τ Yukawa couplings by y_t, y_b and y_τ, respectively. Models that contribute to m_W in such a way that they cannot improve upon the SM fit are greyed out.*
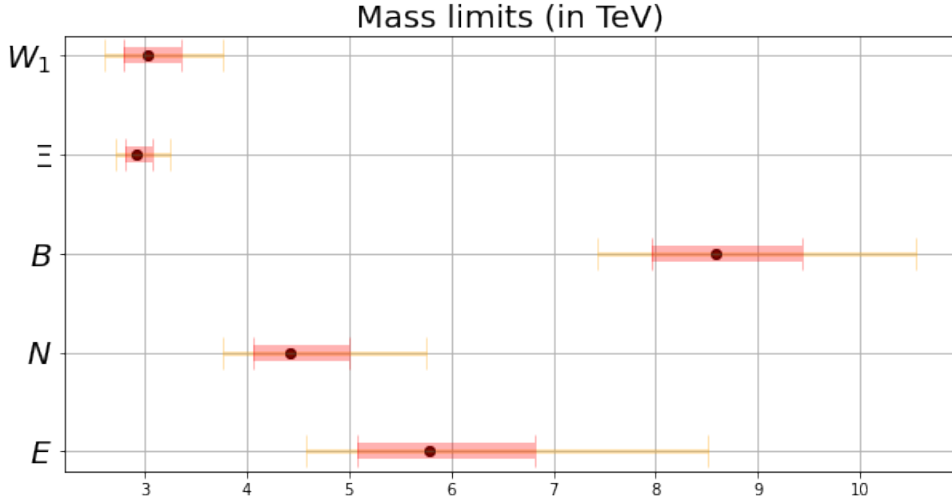

Figure 6. *The horizontal bars show the mass limits (in TeV) at the 68 and 95% CL for the models described in Table 2, setting the corresponding couplings to unity. A larger (smaller) coupling would increase (decrease) the mass ranges proportionally. The coupling limits obtained when setting the mass to 1 TeV are listed in Table 4.*

made the simplifying choice of fixing $\kappa_\Xi = 1$ TeV, although we note that another, equally simple choice could be to set $\kappa_\Xi = M_\Xi$, in which case the results become identical to those of the B model.

The three single-field extensions of the SM that fit best the CDF and other data are

models W_1, B and Ξ, which are all SU(3) singlets and SU(2) triplets, but differ in their spins and hypercharge (spin 1 with unit hypercharge, spin 1 with zero hypercharge, and spin 0 with zero hypercharge, respectively). Each of these models exerts a pull of about 6.4 relative to the SM. The next best model is N, which is a singlet fermion, also known as a sterile neutrino or heavy neutral lepton, which is a zero-hypercharge singlet of both SU(3) and SU(2). This model exerts a pull of about 5 relative to the SM. Finally, we note that model E, which is a singlet fermion with non-zero hypercharge, exerts a pull of about 3.5. These are the models in Table 3 that generate non-zero coefficients for either $C_{Hl}^{(3)}$ or C_{HD} with the negative sign that is indicated by the individual fits in Fig. 3. The other single-field extensions do not improve upon the SM fit, either because they do not contribute to either of these operator coefficients, or because their contributions have the disfavoured sign. Table 4 lists the central values and 68% and 95% CL ranges of the masses of the extra fields that give better fits than the SM, assuming that their couplings are unity, and the 68% CL ranges of their couplings, assuming a mass of 1 TeV. We see that if the coupling in one of these models is of order unity the mass is large enough for the leading-order SMEFT analysis employed here to be consistent, and this would probably be the case even if the coupling were $\mathcal{O}(0.1)$.

Model	Pull	Best-fit mass (TeV)	1-σ mass range (TeV)	2-σ mass range (TeV)	1-σ coupling^2 range
W_1	6.4	3.0	[2.8, 3.6]	[2.6, 3.8]	[0.09, 0.13]
B	6.4	8.6	[8.0, 9.4]	[7.4, 10.6]	[0.011, 0.016]
Ξ	6.4	2.9	[2.8, 3.1]	[2.7, 3.2]	[0.011, 0.016]
N	5.1	4.4	[4.1, 5.0]	[3.8, 5.8]	[0.040, 0.060]
E	3.5	5.8	[5.1, 6.8]	[4.6, 8.5]	[0.022, 0.039]

Table 4. *Single-field models that can improve on the SM fit when the CDF measurement of m_W is included, showing their respective pulls, the best-fit masses and their 1- and 2-σ ranges assuming unit couplings, and the 1-σ coupling ranges assuming masses of 1 TeV.*

We have analysed the effect on this analysis of applying the PDG recommendation [32] for rescaling the stated uncertainties when combining measurements that are only poorly consistent. The rescaling factor for combining the various m_W measurements shown in Fig. 1 is a factor ~ 2, and leads to the revised numbers for the preferred parameter ranges for single-field extensions of the SM shown in Table 5. In general, the pulls for the single-field extensions are reduced, as one would expect. The best-fit masses for the bosonic models W_1, B and Ξ are not changed substantially, increasing by $\sim 1\sigma$ in each case, but there are larger changes in the best-fit masses for the fermionic models N and E. The changes in the 1- and 2-σ parameter ranges for the different models reflect these effects.

5   Prospects for Direct Detection of New Particles at the LHC

The single-field extension that gives the best fit, W_1, is an isospin triplet vector boson with non-zero hypercharge, which is not a common feature of unified gauge theories. The

Model	Pull	Best-fit mass (TeV)	1-σ mass range (TeV)	2-σ mass range (TeV)	1-σ coupling^2 range
W_1	2.8	3.3	[2.9, 4.3]	[2.6, 3.8]	[0.06, 0.12]
B	2.8	10.0	[8.2, 12.0]	[7.4, 10.6]	[0.007, 0.015]
Ξ	2.8	3.1	[2.9, 3.5]	[2.7, 3.3]	[0.007, 0.015]
N	2.1	6.5	[5.1, 8.6]	[4.6, 20.8]	[0.013, 0.038]
E	0.6	13.6	[8.1, 29.7]	[6.3, ∞)	[0.001, 0.015]

Table 5. *As Table 4, but applying the PDG recommendation [32] for rescaling the stated uncertainties when combining measurements that are only poorly consistent.*

next-best fit introduces B, a singlet vector boson with zero hypercharge, commonly known as a Z', which was shown previously to be able to increase the W mass [39, 40], and Ξ, a spin-zero isotriplet boson with zero hypercharge, which is a type of field that appears in some extended Higgs sectors (see, e.g., [38]). Among the other fields that could improve on the SM fit, N and E are singlet fermions with zero and non-zero hypercharges, respectively, and the N field could be identified with a singlet heavy neutral lepton.

The particles that could best explain the new W mass measurement, the vector and scalar triplets W_1 and Ξ would have masses around 3 TeV for a coupling of $\mathcal{O}(1)$ and 1 TeV, respectively. In such a case these particles would be kinematically accessible at the LHC, with a guaranteed production mechanism via their electroweak couplings. Moreover, as the SMEFT constrains only the ratio of coupling to mass, masses below the TeV scale would be favoured in a weak coupling scenario. On the other hand, the best fit for the vector B mass is around 8.6 TeV for an $\mathcal{O}(1)$ coupling, making this option less interesting from the direct search point of view.

We note that, among all the possible interactions these new particles could have, our analysis is sensitive only to the coupling to the electroweak symmetry-breaking sector, e.g., the triplet coupling $\kappa_\Xi\, H^\dagger\, \Xi^a \sigma^a H$. Heavy triplets would be produced in pairs, or produced singly in vector-boson fusion (VBF) with a suppression by the ratio of the vevs of the triplet and doublet, v_t/v. The triplet would then decay to bosons if kinematically allowed, see, e.g., Refs. [49] and [50] for studies of the collider phenomenologies of real and complex scalar triplets. In more complete scenarios such as supersymmetry or the Georgi-Machacek model [51], the triplet would be accompanied by other new particles and exhibit a richer phenomenology, including a candidate for dark matter, see, e.g., Ref. [52] for a recent study in the context of supersymmetry.

There have been various searches for heavy charged Higgses that apply to the Ξ scenario. For example, CMS has performed a VBF search in WW and WZ final states with the full Run 2 dataset [53]. Their search is sensitive to $\sigma \times Br \sim \mathcal{O}(\text{few fb})$ in the mass range 1-3 TeV, right in the ballpark of the preferred region from the SMEFT fit. The phenomenology of B, also known as a Z', is well understood, but searches often focus on possible couplings to light fermions through their $U(1)'$ charges and/or mixing with the SM gauge bosons. On the other hand, if we rely just on the coupling to the Higgs sector, the primary phenomenological

consequence is the presence of $Z - Z'$ mass-mixing. This leads to the heavy gauge boson inheriting the couplings of the Z-boson, suppressed by the mixing angle $\sim \hat{g}_H^B v^2 / M_B^2$ [54]. Its production and decay modes would therefore be similar to the Z itself. We estimate that, for $\hat{g}_H^B \sim \mathcal{O}(1)$, current LHC searches for dilepton resonances are only sensitive to $M_B \sim 1.5$ TeV [55], suggesting that it will be challenging for the LHC to probe the viable parameter space of this simplified scenario.

Interpreting existing direct collider searches for W_1, the vector triplet with hypercharge $Y = 1$, is not as straightforward as for the Ξ particle. Whereas there have been studies on the phenomenology of $Y = 0$ vector triplets, see e.g. Refs. [56, 57], the translation of these limits into the new scenario would require developing a tailored search strategy. Currently, LHC searches are interpreted within various benchmark scenarios [58]: a scenario where the couplings to fermions and gauge bosons are of the same order, a mass-suppressed fermion couplings scenario as in composite Higgs Models, and a purely-bosonic coupling scenario. In the first two cases, searches for a ZH final state are nowadays sensitive to $\sigma \times Br \lesssim \mathcal{O}(1 \text{ fb})$ in the mass range 2-5 TeV. On the other hand, the case of a purely-bosonic state is similar to the situation described above for the scalar triplet, where the production is via VBF and the final state contains massive bosons.

6   Conclusions

The recent CDF measurement of m_W poses a strong challenge, not only to the Standard Model, but also to many well-studied extensions such as supersymmetry [37]. However, we have shown that it is compatible with a general leading-order dimension-6 SMEFT analysis: new physics parametrised by dimension-6 operators can generically account for a large enough shift in m_W without any significant tension with other electroweak precision, Higgs and diboson data.

Table 6 summarises the qualities of SMEFT fits that we find under various assumptions, either without using any m_W measurement, or using only the measurements prior to the recent CDF measurement, or combining the CDF measurement with previous measurements. We present the qualities of fits using the full set of 20 dimension-6 SMEFT operators and restricting to only the 4 operators that can increase m_W relative to its SM value. We see that in all cases the $\chi^2/\text{dof} < 1$ and the p-values are > 0.5, indicating high levels of consistency with the data.

We have also used the SMEFT to show that the CDF and other m_W measurements can be accommodated within several single-field extensions of the Standard Model with new particles whose masses are in the TeV range for couplings of order unity, in which case the SMEFT approach is self-consistent. We find the strongest pulls for an electroweak triplet, either scalar or vector with zero or unit hypercharge respectively, a singlet Z' vector boson, followed by a singlet heavy neutral lepton. The LHC searches made so far have not excluded particles with masses and couplings in the favoured ranges, but there are prospects for LHC Run 3 and HL-LHC that merit more detailed study.

EWPO, H diboson	Previous m_W	Combined m_W	Parameter Count	N_{dof}	χ^2/dof	p-value
✓			20	182	0.92	0.76
✓	✓		20	185	0.93	0.75
✓		✓	20	185	0.97	0.59
✓			4	198	0.93	0.76
✓	✓		4	201	0.93	0.75
✓		✓	4	201	0.97	0.60

Table 6. *Fits to the electroweak, Higgs and diboson data either without any m_W measurement, or with the measurements prior to the recent CDF measurement, or with the combination of the CDF and previous measurements, using either the full set of 20 SMEFT operators or only the 4 operators that can increase m_W relative to its SM value.*

Note Added

As we were completing this paper, several papers [59–66] appeared that also discuss the impact of the new m_W measurement on new physics scenarios.

Ref. [66] is the most similar in spirit to our work, in that it also reports results from fits to oblique observables and a SMEFT fit, though only to electroweak precision observables and without specific model interpretations. Ref. [64] also discusses oblique observables and considers interpretations invoking heavy Z' bosons, little-Higgs models or higher-dimensional geometries. Refs [59–61] discuss two-Higgs doublet models, Ref. [62] proposes a leptoquark interpretation that also accommodates $g_\mu - 2$, Ref [63] considers various models with light degrees of freedom, and Ref. [65] discusses a supersymmetric interpretation.

Acknowledgments

A   Constraints from CKM unitarity

It was pointed out in Refs. [67, 68] that the consistency of β-decay measurements with the unitarity of the Cabibbo-Kobayashi-Maskawa (CKM) quark mixing matrix imposes a sig-
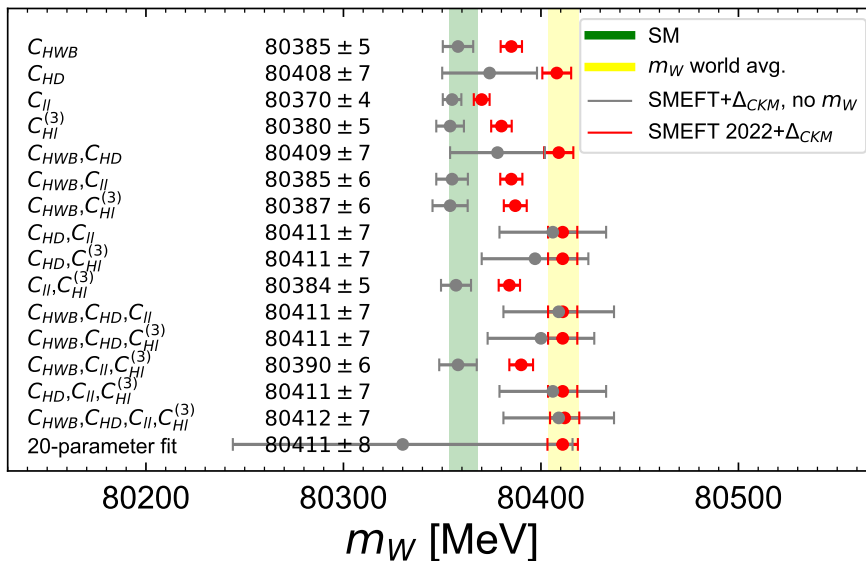
Figure 7. *Values of m_W in fits including all combinations of operators entering linearly in m_W, including from 1 to 4 operator ceofficients, as well as a fit to 20 operator coefficients. Results omitting direct measurements of m_W but including Δ_{CKM} are shown in grey, and results with Δ_{CKM} and using the current world average of m_W measurements including that by CDF are shown in red. The vertical green band is the SM prediction for m_W based on a SM electroweak fit excuding m_W and Δ_{CKM}, and the yellow band is the current world average of m_W measurements.*

nificant constraint on one combination of the dimension-6 SMEFT coefficients. Specifically, the quantity $\Delta_{CKM} \equiv |V_{ud}|^2 + |V_{us}|^2 - 1$ can be expressed as

$$\Delta_{CKM} = 2\frac{v^2}{\Lambda^2}\left[C_{Hq}^{(3)} - C_{H\ell}^{(3)} + C_{\ell\ell} - C_{\ell q}^{(3)} \right],\tag{A.1}$$

and measurements of $0^+ \rightarrow 0^+$ nuclear transitions and kaon decays indicate that

$$\Delta_{CKM} = -0.0015 \pm 0.0007,\tag{A.2}$$

which is consistent with CKM unitarity at the per mille level. In this appendix we discuss the impact of including this measurement in our fit, leaving a more complete study of low-energy measurements to future work.

We note that two of the operators listed in (A.1) that contribute to Δ_{CKM} also contribute to m_W, namely $C_{H\ell}^{(3)}$ and $C_{\ell\ell}$, whereas the other two operators that contribute to Δ_{CKM}, namely $C_{Hq}^{(3)}$ and $C_{\ell q}^{(3)}$, do not contribute to m_W. Conversely, whereas C_{HWB} and C_{HD} contribute to m_W, they do not contribute to Δ_{CKM}. The upshot of this summary is that the CKM unitarity constraint (A.2) is irrelevant for the coefficients of the operators $\mathcal{O}_{HWB}$ and $\mathcal{O}_{HD}$, but is potentially important for $\mathcal{O}_{H\ell}^{(3)}$ and $\mathcal{O}_{\ell\ell}$. Two scenarios can be distinguished, either $C_{H\ell}^{(3)} = C_{\ell\ell}$, in which case the constraints on the non-m_W operator coefficients $C_{Hq}^{(3)}$ and $C_{\ell q}^{(3)}$ can be considered separately, or there is no cancellation between
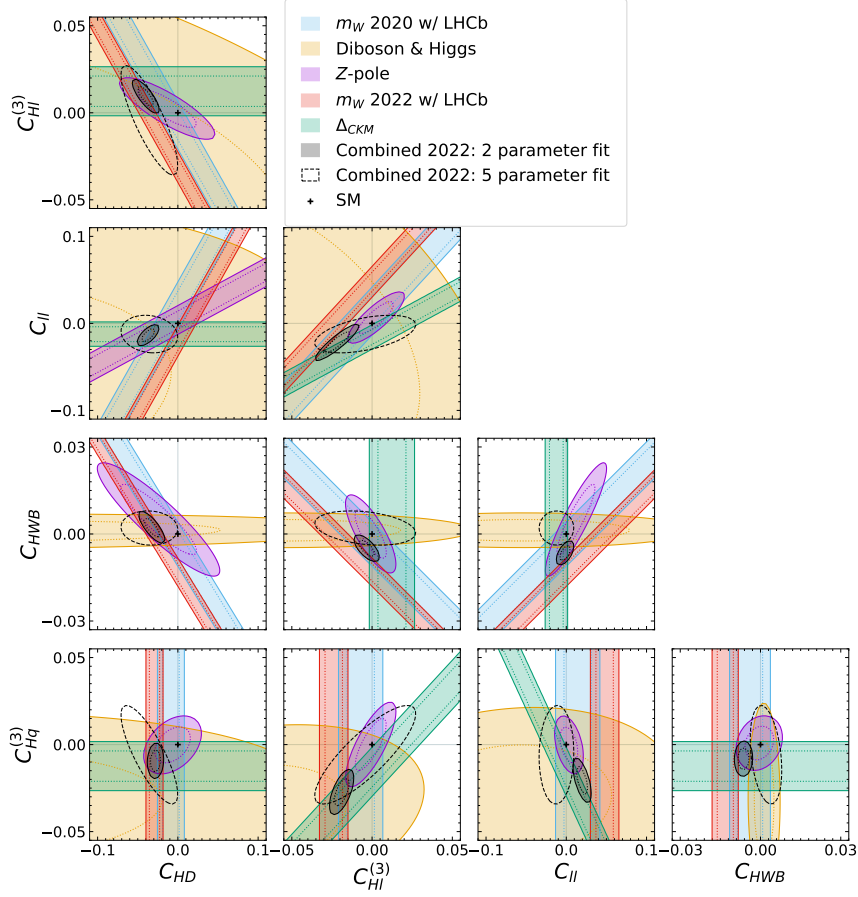
Figure 8. *Planes of pairs of coefficients of operators that can affect m_W and Δ_{CKM}, showing the constraints from direct m_W measurements before (blue) and after (red) the recent CDF update, Z-pole data (purple), diboson and Higgs data (beige), and Δ_{CKM} (green). The combined constraints are given by solid and dashed dotted lines for a 2- and 5-parameter fit respectively.*

EWPO, H diboson	Previous m_W	Combined m_W	Δ_{CKM}	Parameter Count	N_{dof}	$\chi^2/$dof	p-value
✓			✓	20	183	0.94	0.71
✓	✓		✓	20	186	0.93	0.74
✓		✓	✓	20	186	0.98	0.56
✓			✓	4	199	0.93	0.74
✓	✓		✓	4	202	0.93	0.75
✓		✓	✓	4	202	0.97	0.62

Table 7. *As Table 6, but including also the Δ_{CKM} constraint.*

$C_{H\ell}^{(3)}$ and $C_{\ell\ell}$, in which case all four of the operator coefficients in (A.1) must be considered together.

Fig. 7 shows the m_W values in grey corresponding to the best fit and 1-σ range allowed by our fit to various coefficient subsets of the SMEFT without including direct m_W measurements, but with the constraint from Δ_{CKM}. Comparing to Fig. 4, we see that flat directions involving C_{HD} and C_{ll} are lifted by including Δ_{CKM}, giving indirect predictions for m_W compatible with the world average of the direct measurements, which is represented by the yellow band. This is further illustrated in Fig. 8, where two-dimensional contours corresponding to the constraints from various measurements are plotted for all combinations of the 5 parameters $C_{HD}, C_{Hl}^{(3)}, C_{ll}, C_{HWB}, C_{Hq}^{(3)}$. The flat direction for C_{ll} vs C_{HD} corresponding to the Z-pole data in purple can be removed by either including direct m_W measurements, shown before (blue) and after (red) the latest CDF measurement, or by including Δ_{CKM} in green. We note also in beige the importance of diboson and Higgs data for constraining the C_{HWB} operator. The solid black and dashed black ellipses correspond to the combined bounds for the 2-parameter and marginalised 5-parameter fits respectively.

Turning now to the impact of Δ_{CKM} on the single-field extensions of the SM studied here, we note that none of them contribute to C_{HWB}, whereas models B, Ξ and W_1 contribute to C_{HD} with the appropriate sign to increase m_W and are not constrained by CKM unitarity. Models N and E also contribute to m_W with the appropriate sign, and also to $C_{H\ell}^{(3)}$ but not $C_{\ell\ell}$. Hence the CKM unitarity constraint is relevant to these models, but it may be satisfied by contributions from $C_{Hq}^{(3)}$ and $C_{\ell q}^{(3)}$. It seems likely that the current constraints on these coefficients from a global SMEFT fit are weak enough to cancel the $C_{H\ell}^{(3)}$ contribution to Δ_{CKM} to the level needed.

Finally, in Table 7 we summarise the χ^2 per degree of freedom and p-values for our 20- and 4-parameter global fits including Δ_{CKM}, both without and together with m_W measurements before and after the latest CDF result. We again see that in all cases the p-values indicate high levels of consistency with the data.

References

[1] S. Weinberg, *Baryon and Lepton Nonconserving Processes, Phys. Rev. Lett.* **43** (1979) 1566–1570.

[2] W. Buchmuller and D. Wyler, *Effective Lagrangian Analysis of New Interactions and Flavor Conservation, Nucl. Phys. B* **268** (1986) 621–653.

[3] J. Ellis, M. Madigan, K. Mimasu, V. Sanz, and T. You, *Top, Higgs, Diboson and Electroweak Fit to the Standard Model Effective Field Theory, JHEP* **04** (2021) 279, [arXiv:2012.02779].

[4] **LHCb** Collaboration, R. Aaij et al., *Test of lepton universality in beauty-quark decays, Nature Phys.* **18** (2022), no. 3 277–282, [arXiv:2103.11769].

[5] **Muon g-2** Collaboration, G. W. Bennett et al., *Final Report of the Muon E821 Anomalous Magnetic Moment Measurement at BNL, Phys. Rev. D* **73** (2006) 072003, [hep-ex/0602035].

[6] **Muon g-2** Collaboration, B. Abi et al., *Measurement of the Positive Muon Anomalous Magnetic Moment to 0.46 ppm, Phys. Rev. Lett.* **126** (2021), no. 14 141801, [arXiv:2104.03281].

[7] **SMEFiT** Collaboration, J. J. Ethier, G. Magni, F. Maltoni, L. Mantani, E. R. Nocera, J. Rojo, E. Slade, E. Vryonidou, and C. Zhang, *Combined SMEFT interpretation of Higgs, diboson, and top quark data from the LHC*, JHEP **11** (2021) 089, [arXiv:2105.00006].

[8] J. Ellis, C. W. Murphy, V. Sanz, and T. You, *Updated Global SMEFT Fit to Higgs, Diboson and Electroweak Data*, JHEP **06** (2018) 146, [arXiv:1803.03252].

[9] E. da Silva Almeida, A. Alves, N. Rosa Agostinho, O. J. P. Éboli, and M. C. Gonzalez-Garcia, *Electroweak Sector Under Scrutiny: A Combined Analysis of LHC and Electroweak Precision Data*, Phys. Rev. D **99** (2019), no. 3 033001, [arXiv:1812.01009].

[10] A. Biekoetter, T. Corbett, and T. Plehn, *The Gauge-Higgs Legacy of the LHC Run II*, SciPost Phys. **6** (2019), no. 6 064, [arXiv:1812.07587].

[11] A. Falkowski and D. Straub, *Flavourful SMEFT likelihood for Higgs and electroweak data*, JHEP **04** (2020) 066, [arXiv:1911.07866].

[12] J. J. Ethier, R. Gomez-Ambrosio, G. Magni, and J. Rojo, *SMEFT analysis of vector boson scattering and diboson data from the LHC Run II*, Eur. Phys. J. C **81** (2021), no. 6 560, [arXiv:2101.03180].

[13] E. d. S. Almeida, A. Alves, O. J. P. Éboli, and M. C. Gonzalez-Garcia, *Electroweak legacy of the LHC run II*, Phys. Rev. D **105** (2022), no. 1 013006, [arXiv:2108.04828].

[14] S. Iranipour and M. Ubiali, *A new generation of simultaneous fits to LHC data using deep learning*, JHEP **05** (2022) 032, [arXiv:2201.07240].

[15] S. Dawson and P. P. Giardino, *Flavorful electroweak precision observables in the Standard Model effective field theory*, Phys. Rev. D **105** (2022), no. 7 073006, [arXiv:2201.09887].

[16] A. Buckley, C. Englert, J. Ferrando, D. J. Miller, L. Moore, M. Russell, and C. D. White, *Constraining top quark effective theory in the LHC Run II era*, JHEP **04** (2016) 015, [arXiv:1512.03360].

[17] N. P. Hartland, F. Maltoni, E. R. Nocera, J. Rojo, E. Slade, E. Vryonidou, and C. Zhang, *A Monte Carlo global analysis of the Standard Model Effective Field Theory: the top quark sector*, JHEP **04** (2019) 100, [arXiv:1901.05965].

[18] S. van Beek, E. R. Nocera, J. Rojo, and E. Slade, *Constraining the SMEFT with Bayesian reweighting*, SciPost Phys. **7** (2019), no. 5 070, [arXiv:1906.05296].

[19] G. Durieux, A. Irles, V. Miralles, A. Peñuelas, R. Pöschl, M. Perelló, and M. Vos, *The electro-weak couplings of the top and bottom quarks – global fit and future prospects*, JHEP **12** (2019) 098, [arXiv:1907.10619].

[20] S. Bißmann, J. Erdmann, C. Grunwald, G. Hiller, and K. Kröninger, *Constraining top-quark couplings combining top-quark and **B** decay observables*, Eur. Phys. J. C **80** (2020), no. 2 136, [arXiv:1909.13632].

[21] I. Brivio, S. Bruggisser, F. Maltoni, R. Moutafis, T. Plehn, E. Vryonidou, S. Westhoff, and C. Zhang, *O new physics, where art thou? A global search in the top sector*, JHEP **02** (2020) 131, [arXiv:1910.03606].

[22] **CMS** Collaboration, *Using associated top quark production to probe for new physics within the framework of effective field theory*, CMS-PAS-TOP-19-001 (2020).

[23] S. Bißmann, C. Grunwald, G. Hiller, and K. Kröninger, *Top and Beauty synergies in SMEFT-fits at present and future colliders*, JHEP **06** (2021) 010, [arXiv:2012.10456].

[24] S. Bruggisser, R. Schäfer, D. van Dyk, and S. Westhoff, *The Flavor of UV Physics*, JHEP **05** (2021) 257, [arXiv:2101.07273].

[25] V. Miralles, M. M. López, M. M. Llácer, A. Peñuelas, M. Perelló, and M. Vos, *The top quark electro-weak couplings after LHC Run 2*, JHEP **02** (2022) 032, [arXiv:2107.13917].

[26] L. Alasfar, J. de Blas, and R. Gröber, *Higgs probes of top quark contact interactions and their interplay with the Higgs self-coupling*, JHEP **05** (2022) 111, [arXiv:2202.02333].

[27] Y. Liu, Y. Wang, C. Zhang, L. Zhang, and J. Gu, *Probing Top-quark Operators with Precision Electroweak Measurements*, arXiv:2205.05655.

[28] **CDF** Collaboration, T. Aaltonen et al., *High-precision measurement of the W boson mass with the CDF II detector*, Science **376** (2022), no. 6589 170–176.

[29] **ALEPH, DELPHI, L3, OPAL, SLD, LEP Electroweak Working Group, SLD Electroweak Group, SLD Heavy Flavour Group** Collaboration, S. Schael et al., *Precision electroweak measurements on the Z resonance*, Phys. Rept. **427** (2006) 257–454, [hep-ex/0509008].

[30] **D0** Collaboration, V. M. Abazov et al., *Measurement of the W Boson Mass with the D0 Detector*, Phys. Rev. Lett. **108** (2012) 151804, [arXiv:1203.0293].

[31] **LHCb** Collaboration, R. Aaij et al., *Measurement of the W boson mass*, JHEP **01** (2022) 036, [arXiv:2109.01113].

[32] **Particle Data Group** Collaboration, C. Patrignani et al., *Review of Particle Physics*, Chin. Phys. C **40** (2016), no. 10 100001.

[33] J. Haller, A. Hoecker, R. Kogler, K. Mönig, T. Peiffer, and J. Stelzer, *Update of the global electroweak fit and constraints on two-Higgs-doublet models*, Eur. Phys. J. C **78** (2018), no. 8 675, [arXiv:1803.01853].

[34] M. E. Peskin and T. Takeuchi, *A New constraint on a strongly interacting Higgs sector*, Phys. Rev. Lett. **65** (1990) 964–967.

[35] G. Altarelli and R. Barbieri, *Vacuum polarization effects of new physics on electroweak processes*, Phys. Lett. B **253** (1991) 161–167.

[36] **ATLAS** Collaboration, M. Aaboud et al., *Measurement of the W-boson mass in pp collisions at $\sqrt{s} = 7$ TeV with the ATLAS detector*, Eur. Phys. J. C **78** (2018), no. 2 110, [arXiv:1701.07240]. [Erratum: Eur.Phys.J.C 78, 898 (2018)].

[37] E. Bagnaschi, M. Chakraborti, S. Heinemeyer, I. Saha, and G. Weiglein, *Interdependence of the new "MUON G-2" Result and the W-Boson Mass*, arXiv:2203.15710.

[38] P. Diessner and G. Weiglein, *Precise prediction for the W boson mass in the MRSSM*, JHEP **07** (2019) 011, [arXiv:1904.03634].

[39] B. C. Allanach, J. E. Camargo-Molina, and J. Davighi, *Global fits of third family hypercharge models to neutral current B-anomalies and electroweak precision observables*, Eur. Phys. J. C **81** (2021), no. 8 721, [arXiv:2103.12056].

[40] M. Algueró, A. Crivellin, C. A. Manzari, and J. Matias, *Importance of $Z - Z'$ Mixing in $b \to s\ell^+\ell^-$ and the W mass*, arXiv:2201.08170.

[41] B. Grzadkowski, M. Iskrzynski, M. Misiak, and J. Rosiek, *Dimension-Six Terms in the Standard Model Lagrangian*, JHEP **10** (2010) 085, [arXiv:1008.4884].

[42] I. Brivio, S. Dawson, J. de Blas, G. Durieux, P. Savard, A. Denner, A. Freitas, C. Hays, B. Pecjak, and A. Vicini, *Electroweak input parameters*, arXiv:2111.12515.

[43] M. Bjørn and M. Trott, *Interpreting W mass measurements in the SMEFT*, *Phys. Lett. B* **762** (2016) 426–431, [arXiv:1606.06502].

[44] A. Falkowski and K. Mimouni, *Model independent constraints on four-lepton operators*, *JHEP* **02** (2016) 086, [arXiv:1511.07434].

[45] A. Falkowski, M. González-Alonso, and K. Mimouni, *Compilation of low-energy constraints on 4-fermion operators in the SMEFT*, *JHEP* **08** (2017) 123, [arXiv:1706.03783].

[46] J. de Blas, J. Criado, M. Perez-Victoria, and J. Santiago, *Effective description of general extensions of the Standard Model: the complete tree-level dictionary*, *JHEP* **03** (2018) 109, [arXiv:1711.10391].

[47] J. de Blas, M. Chala, M. Perez-Victoria, and J. Santiago, *Observable Effects of General New Scalar Particles*, *JHEP* **04** (2015) 078, [arXiv:1412.8480].

[48] T. Felkl, J. Herrero-Garcia, and M. A. Schmidt, *The Singly-Charged Scalar Singlet as the Origin of Neutrino Masses*, *JHEP* **05** (2021) 122, [arXiv:2102.09898].

[49] M. Chabab, M. C. Peyranère, and L. Rahili, *Probing the Higgs sector of $Y = 0$ Higgs Triplet Model at LHC*, *Eur. Phys. J. C* **78** (2018), no. 10 873, [arXiv:1805.00286].

[50] P. Bandyopadhyay and A. Costantini, *Obscure Higgs boson at Colliders*, *Phys. Rev. D* **103** (2021), no. 1 015025, [arXiv:2010.02597].

[51] H. Georgi and M. Machacek, *Doubly Charged Higgs Bosons*, *Nucl. Phys. B* **262** (1985) 463–477.

[52] N. F. Bell, M. J. Dolan, L. S. Friedrich, M. J. Ramsey-Musolf, and R. R. Volkas, *A Real Triplet-Singlet Extended Standard Model: Dark Matter and Collider Phenomenology*, *JHEP* **21** (2020) 098, [arXiv:2010.13376].

[53] **CMS** Collaboration, A. M. Sirunyan et al., *Search for charged Higgs bosons produced in vector boson fusion processes and decaying into vector boson pairs in proton–proton collisions at $\sqrt{s} = 13\,TeV$*, *Eur. Phys. J. C* **81** (2021), no. 8 723, [arXiv:2104.04762].

[54] K. S. Babu, C. F. Kolda, and J. March-Russell, *Implications of generalized Z - Z-prime mixing*, *Phys. Rev. D* **57** (1998) 6788–6792, [[hep-ph/9710441](hep-ph/9710441)].

[55] **ATLAS** Collaboration, G. Aad et al., *Search for high-mass dilepton resonances using 139 fb^{-1} of pp collision data collected at $\sqrt{s} =13\,TeV$ with the ATLAS detector*, *Phys. Lett. B* **796** (2019) 68–87, [arXiv:1903.06248].

[56] J. M. Lizana and M. Perez-Victoria, *Vector triplets at the LHC*, *EPJ Web Conf.* **60** (2013) 17008, [arXiv:1307.2589].

[57] D. Pappadopulo, A. Thamm, R. Torre, and A. Wulzer, *Heavy Vector Triplets: Bridging Theory and Data*, *JHEP* **09** (2014) 060, [arXiv:1402.4431].

[58] **CMS** Collaboration, A. M. Sirunyan et al., *Search for a heavy vector resonance decaying to a Z boson and a Higgs boson in proton-proton collisions at $\sqrt{s} = 13\,TeV$*, *Eur. Phys. J. C* **81** (2021), no. 8 688, [arXiv:2102.08198].

[59] Y.-Z. Fan, T.-P. Tang, Y.-L. S. Tsai, and L. Wu, *Inert Higgs Dark Matter for New CDF W-boson Mass and Detection Prospects*, arXiv:2204.03693.

[60] C.-R. Zhu, M.-Y. Cui, Z.-Q. Xia, Z.-H. Yu, X. Huang, Q. Yuan, and Y. Z. Fan, *GeV antiproton/gamma-ray excesses and the W-boson mass anomaly: three faces of* $\sim 60 - 70$ *GeV dark matter particle?*, arXiv:2204.03767.

[61] C.-T. Lu, L. Wu, Y. Wu, and B. Zhu, *Electroweak Precision Fit and New Physics in light of W Boson Mass*, arXiv:2204.03796.

[62] P. Athron, A. Fowlie, C.-T. Lu, L. Wu, Y. Wu, and B. Zhu, *The W boson Mass and Muon* $g - 2$: *Hadronic Uncertainties or New Physics?*, arXiv:2204.03996.

[63] G.-W. Yuan, L. Zu, L. Feng, and Y.-F. Cai, *W-boson mass anomaly: probing the models of axion-like particle, dark photon and Chameleon dark energy*, arXiv:2204.04183.

[64] A. Strumia, *Interpreting electroweak precision data including the W-mass CDF anomaly*, arXiv:2204.04191.

[65] J. M. Yang and Y. Zhang, *Low energy SUSY confronted with new measurements of W-boson mass and muon g-2*, arXiv:2204.04202.

[66] J. de Blas, M. Pierini, L. Reina, and L. Silvestrini, *Impact of the recent measurements of the top-quark and W-boson masses on electroweak precision fits*, arXiv:2204.04204.

[67] M. Blennow, P. Coloma, E. Fernández-Martínez, and M. González-López, *Right-handed neutrinos and the CDF II anomaly*, arXiv:2204.04559.

[68] V. Cirigliano, W. Dekens, J. de Vries, E. Mereghetti, and T. Tong, *Beta-decay implications for the W-boson mass anomaly*, arXiv:2204.08440.